

The Adsorption Ability of Cibacron Red Dye from Aqueous Solution Using Copper Oxide Nanoparticles

Aya Qasim Khanjar¹  , Ahlam Mohammed Farhan¹  , Ahmed Mahdi Rheima^{*2}  

¹Department of Chemistry, College of Sciences for Women, University of Baghdad, Baghdad, Iraq.

²Department of Chemistry, College of Science, University of Mustansiriyah, Baghdad, Iraq.

*Corresponding Author.

Received 03/10/2022, Revised 08/05/2023, Accepted 10/05/2023, Published Online First 20/11/2023,
Published 1/6/2024



© 2022 The Author(s). Published by College of Science for Women, University of Baghdad.

This is an open-access article distributed under the terms of the [Creative Commons Attribution 4.0 International License](https://creativecommons.org/licenses/by/4.0/), which permits unrestricted use, distribution, and reproduction in any medium, provided the original work is properly cited.

Abstract

This research describes the environmentally friendly production of CuO nanoparticles utilizing watercress plant extract and calcination at 400 C for 3 hours. SEM and TEM were used to analyze the size of nanoparticles. X-ray diffraction (XRD) was used to determine their crystal structure. Energy-dispersive X-ray spectroscopy (EDX) analysis of the created product's structure revealed just copper and oxygen constituents, demonstrating the purity of the synthetic material. The addition of CuO NPs improved the absorption of the dye Cibacron red. At 35 minutes of contact time, quicker adsorption of Cibacron red dye onto CuO nanoparticles was observed. The Freundlich isotherm and kinetic of pseudo-second order with R² values more than 0.9785 and 0.999, respectively, were the most effective in describing the adsorption process. The thermodynamic parameters were calculated using thermodynamic analysis. It can be concluded that CuO NPs are an effective adsorbate surface for the Cibacron red dye.

Keywords: Adsorption, Cibacron red dye, CuO NPs, X-ray diffraction, green synthesis.

Introduction

The creation of materials with unique size, structure, and content is now possible because of nanotechnology ¹, a critical development in contemporary science. Materials with a diameter of less than a nanometer are produced, processed, and used ^{2,3}. Compared to individual bulk atoms and molecules, nanoscale physical, chemical, and biological properties vary ⁴⁻⁶. This makes it possible to develop fresh classes of cutting-edge substances and materials that meet the demands of high-tech applications ⁷⁻¹⁰. Numerous businesses and fields, including as the chemical industry, electrochemical photo applications, environmental health, medicine,

and energy, are using nanotechnology ^{11,12}. Since some time ago, medical institutions have used metal nanoparticles, including gold, silver, and zinc, as therapeutic agents ^{13,14}. In energy, biomedicine, and the environment, transitional metal oxides like CuO, TiO₂, Fe₃O₄, ZnO, and NiO NPs have been successfully used as cutting-edge nanomaterials. These nanoparticles' high adsorption abilities considerably improve their applications and performance ¹⁵⁻¹⁹. There has been increased research into the biological effects of metal nanoparticles. Recently, various researchers began evaluating the biological effects of metal oxide nanoparticles like

copper oxide, whereas increased biological and photocatalytic activities superior to those derived from metal nanoparticles have been observed²⁰⁻²³. CuO NPs have shown unique anticancer, antibacterial, and antioxidant activity in addition to the previously indicated use, making them a viable tool for biomedical applications^{24,25}. Copper oxide nanoparticles have been shown to have potential uses in a variety of fields, including gas sensors, catalysis, solar cells, batteries, food preservation, high temperature superconductors, waste treatment, photovoltaic devices, agriculture, field emission emitters, and dye removal^{26,27}. Dyes, which include all substances used to color textiles, leather, food, and other materials, are regarded as organic pollutants in aqueous systems and may pose a number of risks to all elements of the environment due to their high toxicity, particularly when they are present in high concentrations²⁸. Among the components of industrial effluent, organic compounds play a crucial role. Due to the possibility of some organic contaminants causing malignant diseases, there is a high danger of long-term effects²⁹. According to World Health Organization (WHO) reports, drinking water contamination is the primary source of the majority

of diseases that are spread in underdeveloped nations³⁰. As a result, many treatments have been employed by researchers to treat industrial water³¹. Organic contaminants in industrial water have been treated and eliminated in a variety of ways. They include reverse osmosis, ion exchange, chemical oxidation, photo-oxidation, and the adsorption process³². Adsorption is a technique that is effective and economical. It is frequently used, according to WHO data, to detoxify polluted water³³⁻³⁶. Heterogeneous photocatalytic degradation involves three fundamental processes: surface reaction, ultimate pore and desorption surface adsorption. The adsorption mechanism and reactions were extensively researched using a variety of models and characterization methodologies, depending on the goals of each investigation. However, the fact that the process is optimized is a shared characteristic³⁷. The aim of this research to prepare copper oxide nanoparticles from watercress extract and determine whether CuO nanoparticles could effectively remove the Cibacron red dye, which is one of the dyes used at the textile industry in the Wasit Governorate and the majority of which is disposed of as waste water.

Material and methods

Preparation of Watercress Plant Extract

A plant extract from the watercress has been gathered and cleaned with de-ionized water to remove dust particles. The dry leaves are gently combined in a mixer to create homogenous powders then, 10 g of leaves were pulverized and mixed with 150 ml of de-ionized water, then heated for 30 minutes at 60 °C with stirring. The solution was filtered and stored in the fridge.

Synthesis of CuO Nanoparticles

The green synthesis technique was used to make copper oxide nanoparticles³⁸. In accordance, an amount of 200 ml of watercress extract was added slowly (one drop per second) to 0.01 mole of Cu(NO₃)₂ and stirred for 30 minutes. The green powder was precipitated, separated, and washed with deionized water numerous times. The precipitate was dried for an hour at 150°C and

calcined for three hours at 400°C. The black powder of copper oxide nanoparticles was obtained

Adsorption of Cibacron Red Dye on CuO NPs

The equilibrium isotherm of a particular adsorbent serves as a representation of its adsorbent properties while building adsorption processes. In deionized water, a stock solution of cibacron red dye 50 ppm was created. 10 ml of dye solution were combined with 0.01 g of CuO nanoparticles, which were then heated at 298 K for 30 minutes. A UV-visible absorption spectrophotometer measured the dye concentration after filtering the solution as Eq. 1³⁹.

$$Q_e = (C_0 - C_e)V_{sol}/m \quad 1$$

Where C₀ and C_e are the starting and equilibrium concentrations of Cibacron red dye (mg/L), Q_e (mg/g) is the equilibrium adsorption capacity, and

M is the mass of the CuO nanoparticles (g), V sol is the volume of cibacron red (L).

Characterization of CuO Nanoparticles

The CuO nanoparticles sample was examined using X-ray diffraction (XRD-6000). Transmission

Results and Discussion

The X-ray Diffraction of CuO Nanoparticles

The X-ray crystallography was used to determine the structure of nano-synthesized, in which the crystal's atoms cause an incoming X-ray beam to diffract in various directions. According to XRD analysis, the monoclinic CuO (JCPDS 45-0397) planes (110), (111), (200), (-202), (020), (202), (-113), and (022) are allocated to a series of diffraction peaks at 2θ of 32.41, 35.61, 38.81, 48.91, 53.31, 58.21, 61.61, and 66.31, respectively, Fig. 1. Except for these CuO peaks, all of the diffraction peaks can be indexed as conventional

electron microscopy was used to examine the morphology of nanoparticles. Using a scanning electron microscope (SEM), the CuO nanoparticles' form was examined.

monoclinic structures. No other peaks matching to Cu or Cu₂O were seen. Using the Scherrer formula, the average crystallite size of CuO crystal size was determined as Eq. 2:

$$D = k\lambda / \beta \cos\theta \quad 2$$

where D is the particle size (nm), k is a constant of value 0.94, β is the full-width at half maximum (FWHM) of the peak (in radians), λ is the X-ray wave length 1.5406 Å, as well as 2θ is the Bragg angle (degree). The size of the typical crystallite was determined to be 24nm.

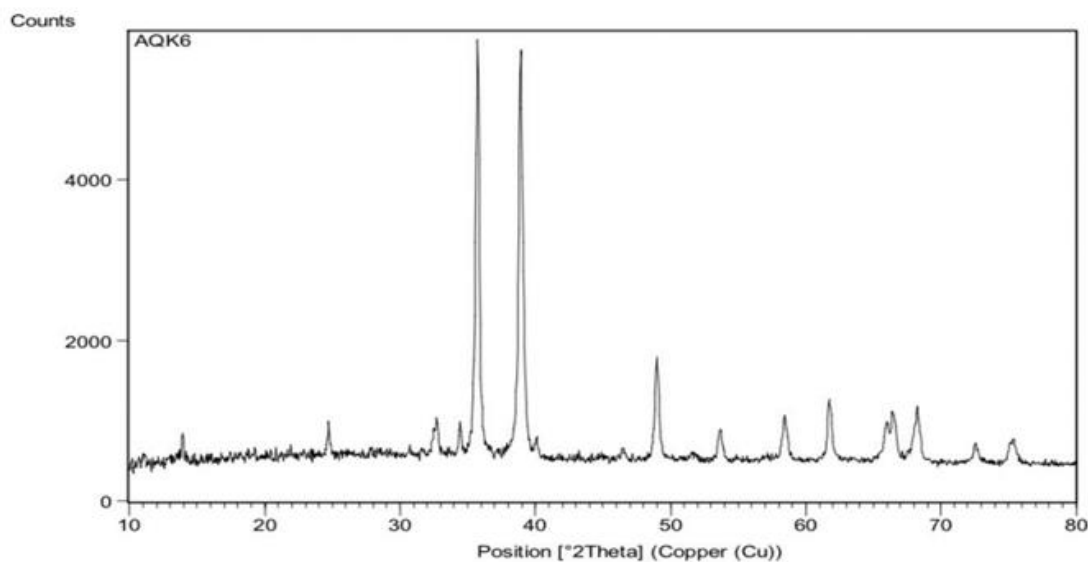


Figure 1. XRD patterns of CuO NPs.

Field Emission Scanning Electron Microscope (FE-SEM)

The surface morphology of pure CuO nanoparticles that had been calcined at 400 °C was examined

using FE-SEM. The prepared sample was produced as semi-spherical aggregates with a roughly uniform distribution, according to the SEM analysis. Equal-sized produced nanoparticles' crystal nature is seen in Fig. 2.

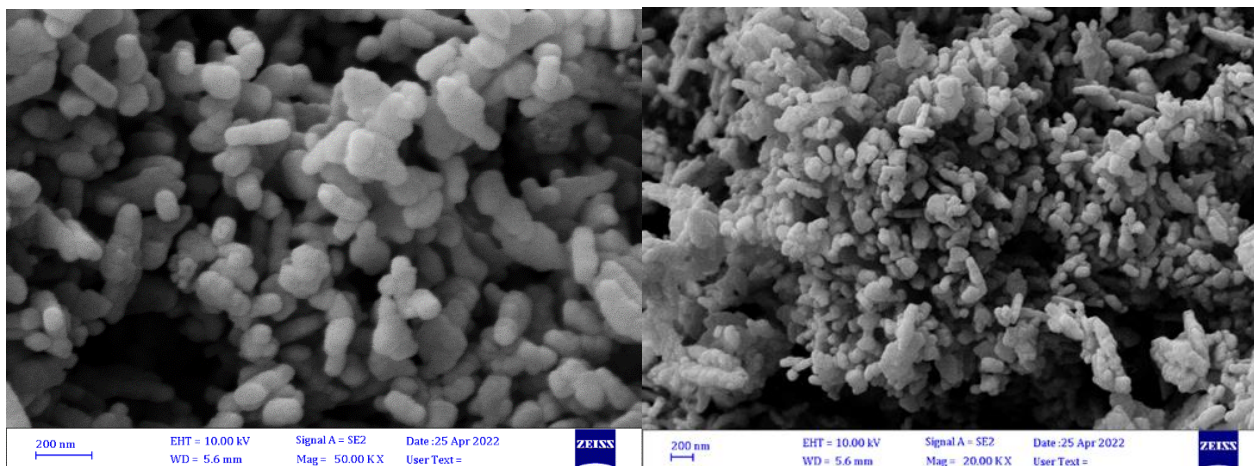


Figure 2. SEM images of the CuO NPs

Transmission Electron Microscopy (TEM)

The TEM image of CuO NPs is depicted in Fig. 3. The TEM image of nanoparticles in various sizes and shapes is depicted in Fig. 3. The TEM examination aims to comprehend the crystalline

properties of the nanoparticles. The particles are determined to be 28 nm in size and to be spherical in shape. The aggregation of tiny nanoparticles into larger ones that have dimensions that match those seen in the XRD study could be the cause of the larger particles ³⁴.

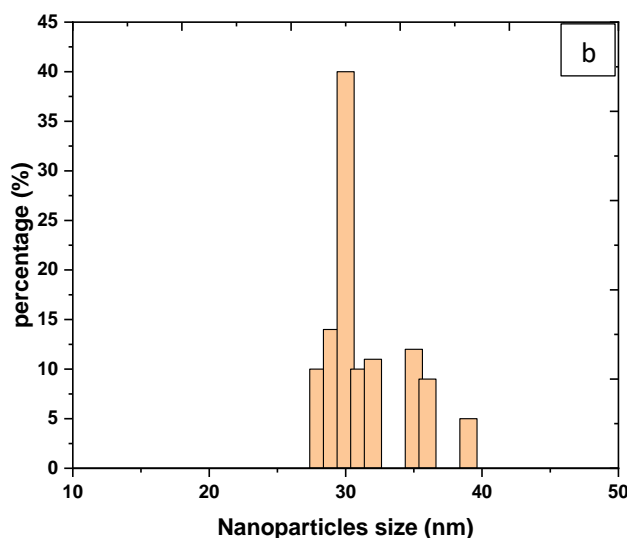
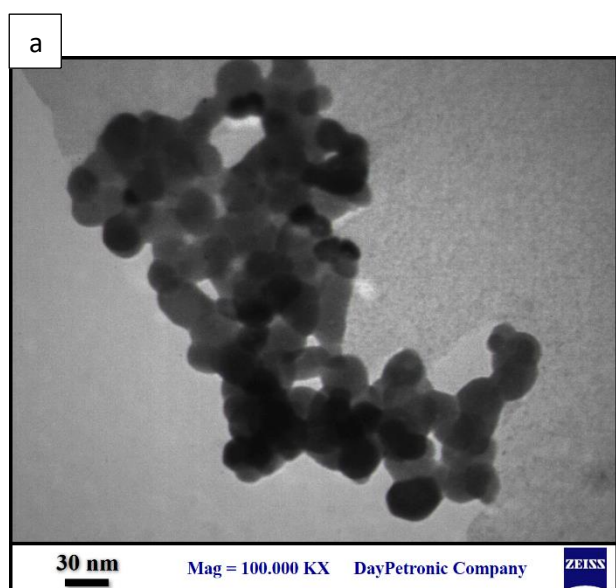


Figure 3. a) TEM images of the CuO NPs and b) distribution of nanoparticles

Energy-dispersive X-ray Spectroscopy Characterization

The EDX spectrum of CuO NPs is depicted in Fig. 4. The spectrum has the usual copper and oxygen peaks. The outcomes support the great purity of the produced nanoparticles. Furthermore, the actual estimations derived from the EDX measurement concur with the theoretical computations of the

elements. The matrix of the mixed catalyst has effectively dispersed the CuO NPs, as shown in Fig. 5. Additional information suggests typical x-ray mapping images that show the distribution of a CuO catalyst's elemental components and facilitate the dispersion of the catalyst's elements.

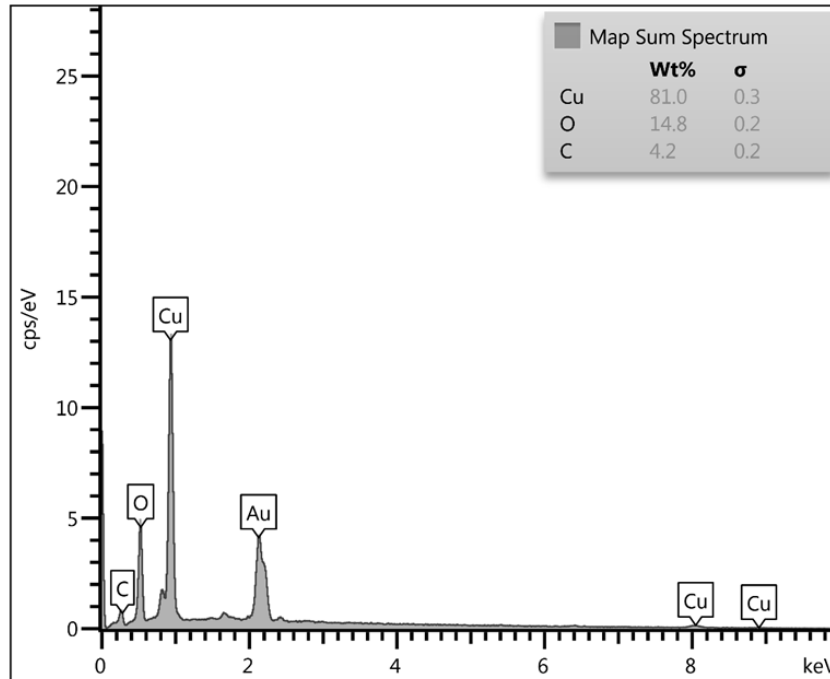


Figure 4. EDX spectrum of CuO NPs

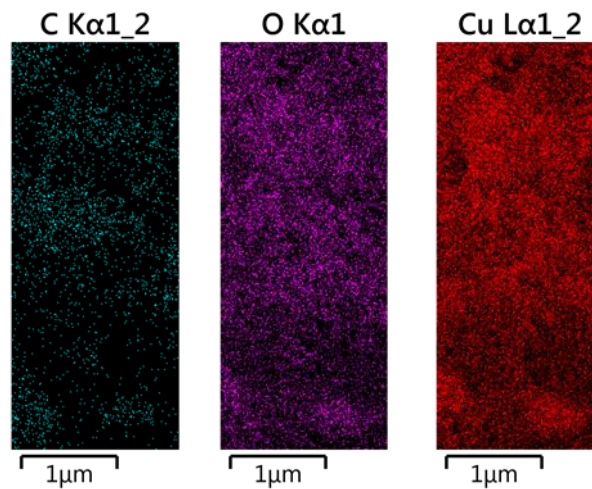


Figure 5. EDAX- mapping of CuO NPs

Adsorption Isotherms

The main objective of the adsorption analysis is to ascertain how the dye and adsorption interact in addition to compare the adsorption isotherm with the adsorption data. The Langmuir and Freundlich models were assessed in this study. The following formula³⁸⁻⁴⁰ describes the linear Freundlich adsorption process as Eq. 3:

$$\log(Q_e) = \log(k_f) + \left(\frac{1}{n}\right) \log(C_e) \quad 3$$

The adsorption capacity, as well as intensity of adsorption, are shown by the Freundlich constants K_f and n , respectively are depicted in Fig. 6. Calculating k_f is done using the intercept, while n is done using the slope. For the CuO isotherm Freundlich, $1/n$ was determined in this work to be 0.235. Thus, this investigation supported the benefit of physical adsorption⁴¹. The adsorption is better fit by the Freundlich isotherm model ($R_2=0.9785$).

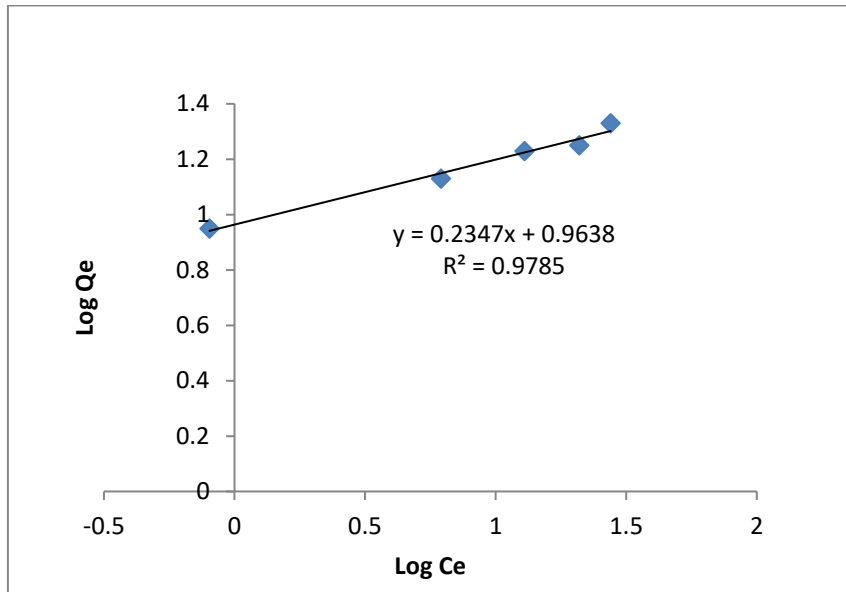


Figure 6. The Freundlich isotherm model plot at 298 K.

The data fits the Langmuir adsorption isotherm (Fig. 7), as can be seen in the Eq. 4, that follows ^{34,40,41}:

$$\frac{C_e}{Q_e} = \frac{1}{q_{max}} K_L + \frac{C_e}{q_{max}} \quad 4$$

The maximum capacity of Cibacron red dye is q_{max} (mg/g), whereas the Langmuir constant is K_L (mg/L). The Langmuir isotherm's key

characteristics are outlined and shown by the separation factor, sometimes referred to this as the dimensionless constant (RL) in Eq. 5 ⁴⁰:

$$RL = \frac{1}{(1 + K_L C_i)} \quad 5$$

The dye adsorbs best on CuO when the initial dye concentration is C_i (mg / L), and the RL values are all within the range of (0–1).

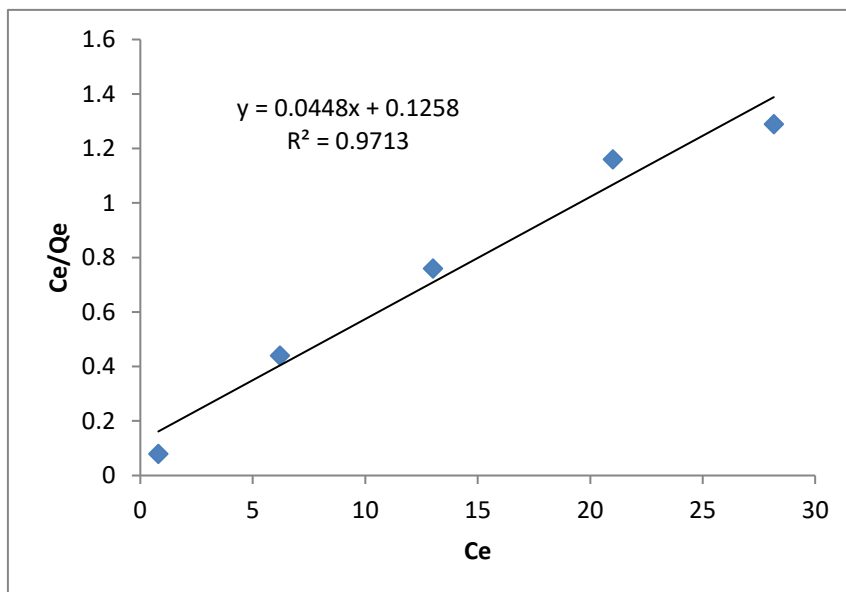


Figure 7. The Langmuir isotherm model at 298 K.

Effect of Contact Time

To measure contact time and equilibrium time, a series of tests using 0.01 g CuO NPs and 10 mL 50 ppm dye were conducted with a 200 rpm shaker at 298 K. The first 5 to 40 minutes of adsorption are

relatively quick. Fast adsorption is made possible by closely associating the active CuO nanoparticles with the dye. As shown in Fig. 8, the nanoparticles' surface causes the dye adsorption rate to stabilize after 30 minutes.

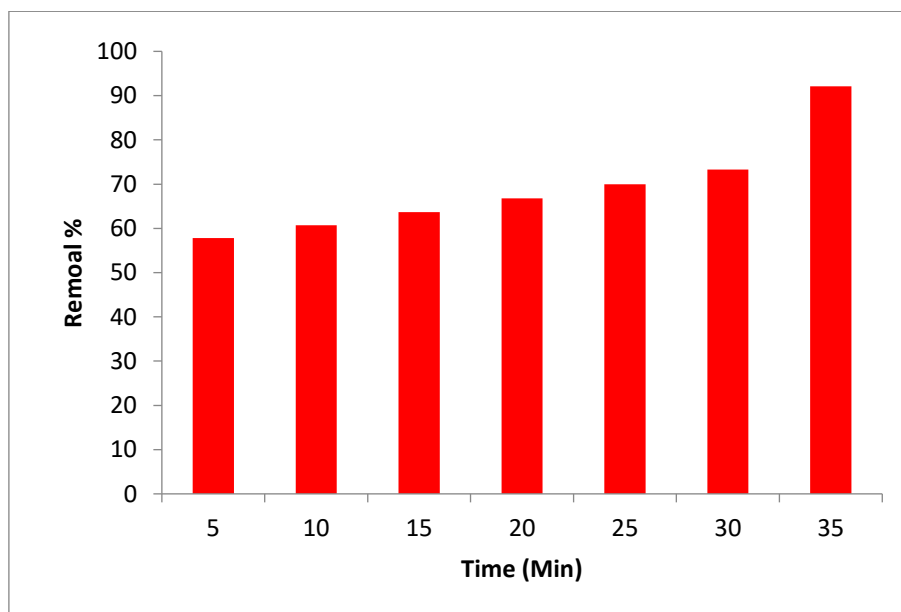


Figure 8. Effect of time on the cibacron dye adsorption onto the CuO NPs.

Effect of Adsorbent Mass

To test the effectiveness of the adsorbent, different masses of CuO NPs 0.005g, 0.01g, 0.05g, 0.1g, and 0.15g were introduced to 50 ppm of dye. Shaking the mixture at 298 K and 200 rpm took place. The

relationship between removal percentage and mass is seen in the graph. Because there are more active sites in nanoparticles, adsorption happens very quickly. Fig. 9, demonstrates the increase in dye adsorption, by boosting the bulk of the CuO NPs.

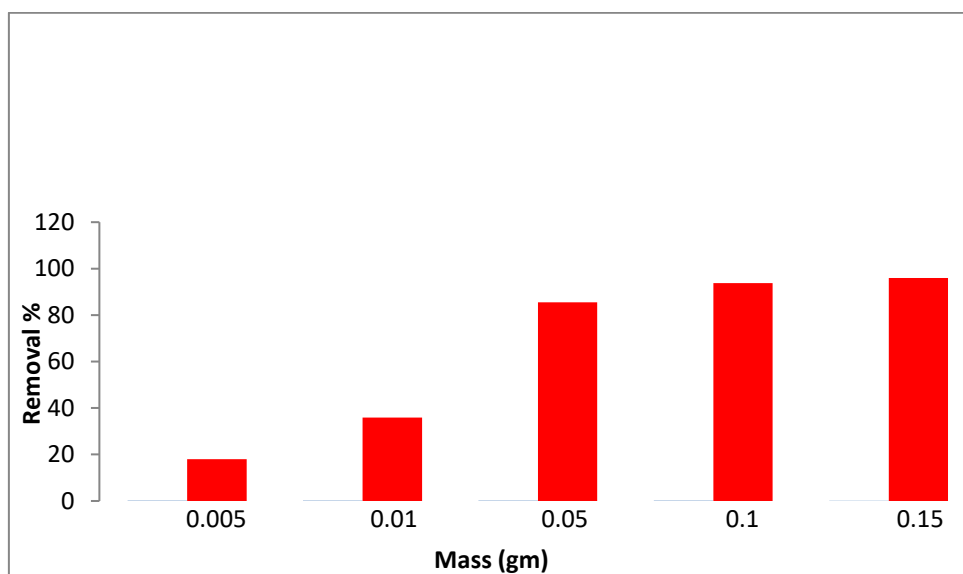


Figure 9. Effect of CuO NPs mass on dye adsorption

Effect of Temperature

The effect of temperature on dye adsorption on the surface of CuO NPs was investigated at several temperatures 288 K to 328 K. As the temperature rises, the dye adsorption solution volume grows. As a result, the endothermic process. This shows how the mechanics of absorption and adsorption work. As the temperature increases, the diffusion rate increases, and a strong bond is formed with the adsorbent. In the perforations, the diffusion molecules are absorbed. The right evaluation of thermodynamic parameters is necessary because they provide accurate information on changes in

inherent energy caused by adsorption. The adsorption free energy (ΔG°), enthalpy (ΔH°) and entropy (ΔS°) were used to analyze the following adjustments to estimate the adsorption process as Eqs. 6-8^{34,40-44}:

$$\ln(Ke) = \frac{-\Delta H}{RT} + \frac{\Delta S}{R} \quad 6$$

$$Ke = \frac{Q_e}{C_e} \quad 7$$

$$\Delta G = \Delta H - T\Delta S \quad 8$$

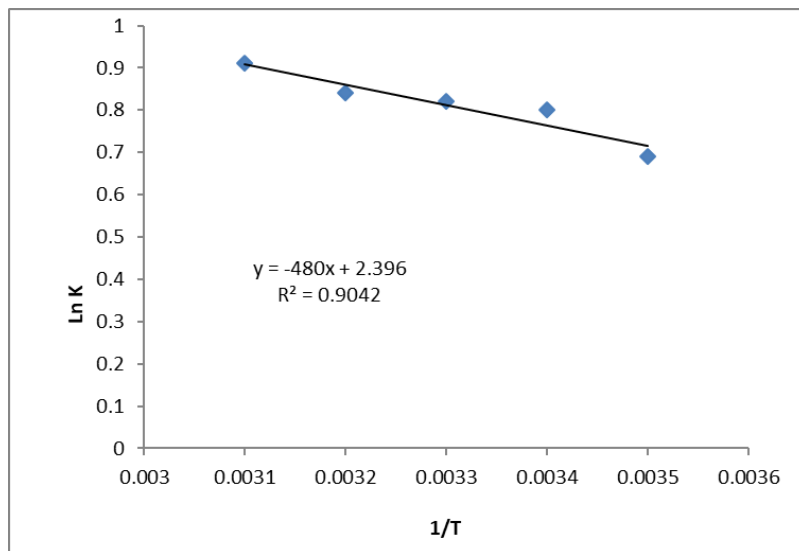


Figure 10. Van't Hoff plot between ln K and 1/T.

Ke is an equilibrium constant, R is gas constant is 8.314 J/mol K, and T is the temperature in Kelvin (K). According to a van't Hoff plot between ln K and 1/T in Fig. 10, the interaction was endothermic and the ΔH was 7.69 kJ/mole determined by slope. The ΔS from the intercept, which was 24.38 J/mole, indicating that the adsorbed particles were still moving close to the surface. With a positive ΔG value of 0.538 KJ/mol at 293 K, non-spontaneous adsorption is implied.

Dynamics

Adsorbent applications depend on the kinetics of dye adsorption on CuO NPs' surface adsorbents. The dye analysis discovered that for 0.01 g of the CuO nanoparticle adsorbents, the adsorption

equilibrium period was approximately 35 minutes. Additionally, in this research, the following information about adsorption was depicted using classical and kinetic models:

Model of pseudo-first-order as Eq. 9^{34,40-44}:

$$\ln(q_e - q_t) = \ln(q_e) - k_1 t \quad 9$$

The equilibrium adsorption capacity, q_e (mg g⁻¹), the amount of dye that has been adsorbed after time, q_t (mg g⁻¹), and k_1 is a pseudo-first-order rate constant (min⁻¹), are shown in Fig. 11. The pseudo-second-order kinetic model is as Eq. 10^{31,32}:

$$\frac{1}{qt} = \frac{1}{k_2 q_e} + \frac{t}{q_e} \quad 10$$

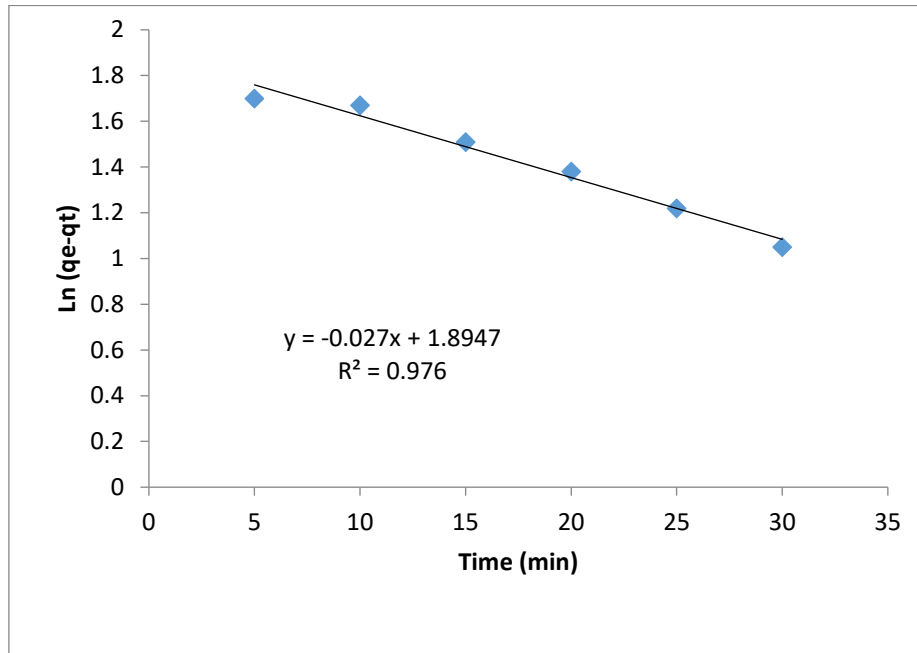


Figure 11. Dynamic of adsorption of dye pseudo-first-order

K_2 is the second-order rate constant. The pseudo-second-order model may adequately describe the

kinetic information with $R_2 = 0.999$, as illustrated in Fig. 12.

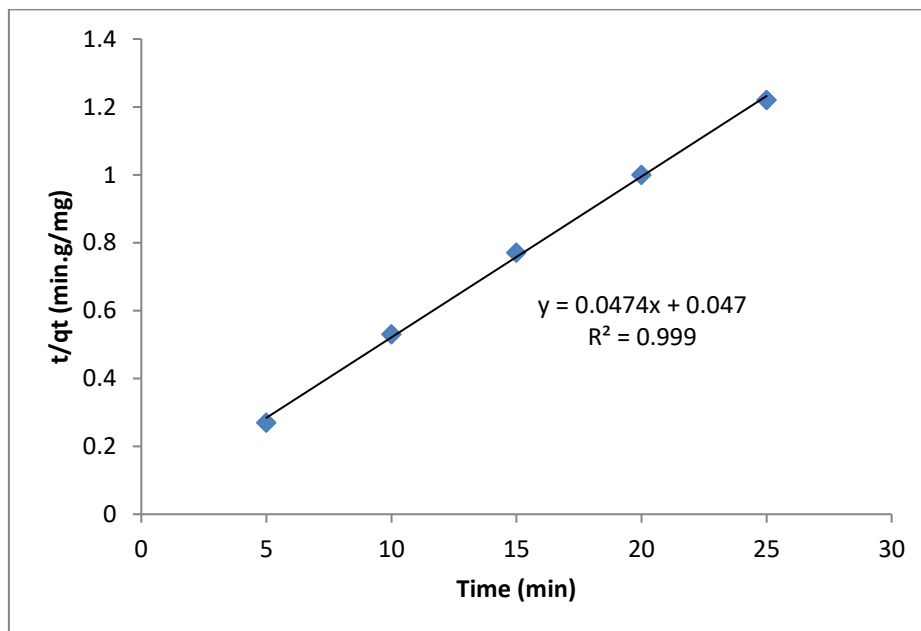


Figure 12. Dynamic of adsorption of dye pseudo-second-order.

Conclusion

Green synthesis and imaging with XRD, SEM/EDX, and TEM were used to create high-quality CuO. According to TEM studies, CuO NPs' particle size ranged from 28 nm. For removing dye from aqueous solutions, the observed adsorption

properties are perfect. In both kinetic and thermodynamic experiments, the usefulness of CuO NPs as adsorbers was proven. Langmuir and Freundlich isotherm models were well-suited to the data. Much better describes the

adsorption is the Freundlich isotherm model. The adsorption is non-spontaneous and endothermic, according to thermodynamics. The slope of the van't Hoff plot was used to determine the enthalpy

value (7.69 kJ/mole), which represents the physical properties of adsorption. This adsorption follows pseudo-second order with $R^2 = 0.999$.

Authors' Declaration

- Conflicts of Interest: None.
- We hereby confirm that all the Figures in the manuscript are ours. Furthermore, any Figures and images, that are not ours, have been

- included with the necessary permission for republication, which is attached to the manuscript.
- Ethical Clearance: The project was approved by the local ethical committee at University of Baghdad.

Authors' Contribution Statement

A.Q.K. was responsible of design, acquisition of data, organized research idea, and contributed to the paper writing. A. M. F. organized research idea and

contributed to the paper writing. A. M. R. conducted the revision and proofreading of the manuscript.

References

1. Noman MT, Amor N, Petru M. Synthesis and applications of ZnO nanostructures (ZONNS): A review. *Crit Rev Solid State Mater Sci.* 2021 Mar 4; 47(2):1-43. <https://doi.org/10.1080/10408436.2021.1886041>.
2. Gonçalves RA, Toledo RP, Joshi N, Berengue OM. Green synthesis and applications of ZnO and TiO₂ nanostructures. *Molecules.* 2021 Apr 13; 26(8): 2236. <https://doi.org/10.3390/molecules26082236>.
3. Shang Y, Hasan MK, Ahammed GJ, Li M, Yin H, Zhou J. Applications of nanotechnology in plant growth and crop protection: a review. *Molecules.* 2019 Jul 13; 24(14): 2558. <https://doi.org/10.3390/molecules24142558>.
4. Zhang J, Terrones M, Park CR, Mukherjee R, Monthieux M, Koratkar N, Kim YS, Hurt R, Frackowiak E, Enoki T, Chen Y. Carbon science in 2016: Status, challenges and perspectives. *Carbon.* 2016 Mar 1; 98(70): 708-32. <http://dx.doi.org/10.1016/j.carbon.2015.11.060>.
5. Aboud N A A, Alkayat WM., Hussain, D H, Rheima AM. A comparative study of ZnO, CuO and a binary mixture of ZnO-CuO with nano-dye on the efficiency of the dye-sensitized solar cell. *J Phys : Conf Ser.* 2020; 1664(1): 012094. <https://doi.org/10.1088/1742-6596/1664/1/012094>.
6. Behl T, Kaur I, Sehgal A, Singh S, Sharma N, Bhatia S, Al-Harrasi A, Bungau S. The dichotomy of nanotechnology as the cutting edge of agriculture: Nano-farming as an asset versus nanotoxicity. *Chemosphere.* 2022 (Feb 1); 288: 132533. <https://doi.org/10.1016/j.chemosphere.2021.132533>.
7. Tian J, Xu J, Zhu F, Lu T, Su C, Ouyang G. Application of nanomaterials in sample preparation. *J Chromatogr. A* 2013 (Jul 26); 1300:2-16. <https://doi.org/10.1016/j.chroma.2013.04.010>.
8. Iqbal SA, Saadiyah AD, Khulood AA, Congo red adsorption on Bentonite and modified Bentonite. *Int interdiscip Res J.* 2013; 3(5): 62-78. <https://api.semanticscholar.org/CorpusID:97190029>.
9. Awaid TJ, Ayal AK, Farhan AM, Sando MS, Chin LY. Effect of electrolyte composition on structural and photoelectrochemical properties of titanium dioxide nanotube arrays synthesized by anodization technique. *Baghdad Sci J.* 2020 Dec 1; 17: 1183. <http://dx.doi.org/10.21123/bsj.2020.17.4.1183>.
10. Al-Haidary Q, Al-Mokaram AM, Ismail AH, Hussein FM. State of the Art of Synthesized PANI-(Sn²⁺/TiO₂) Nanocomposites for Conductive Application. *Al-Mustansiriyah J Sci.* 2022 Mar 10; 33(1): 32-8. <https://doi.org/10.23851/mjs.v33i1.1100>.
11. Kaabipour S, Hemmati S. A review on the green and sustainable synthesis of silver nanoparticles and one-dimensional silver nanostructures. *Beilstein J Nanotechnol.* 2021 Jan 25; 12(1): 102-36. <https://doi.org/10.3762/bjnano.12.9>.
12. Hwaidi AJ, Mohammed NJ. Tuning Structural and Optical Properties of WO₃ NPs Thin Films by the Fluency of Laser Pulses. *Al-Mustansiriyah J Sci.* 2022; 33(3): 94-100. <https://doi.org/10.23851/mjs.v33i3.1145>.
13. Hakeem HS, Abbas NK. Preparing and studying structural and optical properties of Pb_{1-x}Cd_xS nanoparticles of solar cells applications. *Baghdad Sci*

- J. 2021; 18(3): 0640-.
<http://dx.doi.org/10.21123/bsj.2021.18.3.0640>.
14. Li H, Chen X, Shen D, Wu F, Pleixats R, Pan J. Functionalized silica nanoparticles: Classification, synthetic approaches and recent advances in adsorption applications. *Nanoscale*. 2021; 13(38): 15998-6016. <https://doi.org/10.1039/D1NR04048K>.
15. Zinatloo-Ajabshir S, Heidari-Asil SA, Salavati-Niasari M. Rapid and green combustion synthesis of nanocomposites based on Zn-Co-O nanostructures as photocatalysts for enhanced degradation of acid brown 14 contaminant under sunlight. *Sep Purif Technol*. 2022 Jan 1; 280: 119841. <https://doi.org/10.1016/j.seppur.2021.119841>.
16. Waris A, Din M, Ali A, Ali M, Afridi S, Baset A, Khan AU. A comprehensive review of green synthesis of copper oxide nanoparticles and their diverse biomedical applications. *Inorg Chem Commun*. 2021 Jan 1; 123: 108369. <https://doi.org/10.1016/j.inoche.2020.108369>.
17. Letchumanan D, Sok SP, Ibrahim S, Nagoor NH, Arshad NM. Plant-based biosynthesis of copper/copper oxide nanoparticles: an update on their applications in biomedicine, mechanisms, and toxicity. *Biomolecules*. 2021 Apr 12; 11(4): 564. <https://doi.org/10.3390/biom11040564>.
18. Mahmoud AE, Al-Qahtani KM, Alflajj SO, Al-Qahtani SF, Alsamhan FA. Green copper oxide nanoparticles for lead, nickel, and cadmium removal from contaminated water. *Sci Rep*. 2021 Jun 15; 11(1): 1-3. <https://doi.org/10.1038/s41598-021-91093-7>.
19. Shakouly SM. Magnetic Study of BiPbSrCaCuZnO Super Conducting thin film Synthesized by pulsed Laser Deposition (PLD) Method. *Al-Mustansiriyah J Sci*. 2022. Jun 26; 33(2): 77-80. <https://doi.org/10.23851/mjs.v33i2.1045>.
20. Zhang F, Chen X, Wu F, Ji Y. High adsorption capability and selectivity of ZnO nanoparticles for dye removal. *Colloids Surf A: Physicochem. Eng Asp*. 2016 Nov 20; 509: 474-83. <https://doi.org/10.1016/j.colsurfa.2016.09.059>.
21. Ayoman E, Hosseini SG. Synthesis of CuO nanopowders by high-energy ballmilling method and investigation of their catalytic activity on thermal decomposition of ammonium perchlorate particles. *J Therm Anal Calorim*. 2016; 123 : 1213-1224. <https://doi.org/10.1007/s10973-015-5059-1>.
22. Srinivasan M, Venkatesan V, Arumugam G, Natesan N, Saravanan S, Murugesan S, Ramachandran R, Ayyasamy A, Pugazhendhi. Green synthesis and characterization of titanium dioxide nanoparticles (TiO₂ NPs) using *Sesbania grandiflora* and evaluation of toxicity in zebrafish embryos, *Process Biochem*. 2019; 80: 197-202. <https://doi.org/10.1007/s10854-022-09634-3>.
23. Panda SK, Aggarwal I, Kumar H, Prasad L, Kumar A, Sharma A, Vo DV, Van Thuan D, Mishra V. Magnetite nanoparticles as sorbents for dye removal: a review. *Environ Chem. Lett*. 2021 Jun; 19(3): 2487-525. <https://doi.org/10.1007/s10311-020-01173-9>.
24. Ağbulut Ü, Sarıdemir S, Rajak U, Polat F, Afzal A, Verma TN. Effects of high-dosage copper oxide nanoparticles addition in diesel fuel on engine characteristics. *Energy*. 2021 (15); 229: 120611. <https://doi.org/10.1016/j.energy.2021.120611>.
25. Patil VB, Malode SJ, Mangasuli SN, Tuwar SM, Mondal K, Shetti NP. An electrochemical electrode to detect theophylline based on copper oxide nanoparticles composited with graphene oxide. *Micromachines*. 2022 Jul 23; 13(8): 1166. <https://doi.org/10.3390/mi13081166>.
26. Norzaee S, Djahed B, Khaksefidi R, Mostafapour FK. Photocatalytic degradation of aniline in water using CuO nanoparticles, *J Water Supply Res Technol*. 2017; 66 : 178-185. <https://doi.org/10.2166/aqua.2017.104>.
27. Elmer WH, Zuverza-Mena N, Triplett LR, Roberts EL, Silady RA, White JC. Foliar application of copper oxide nanoparticles suppresses Fusarium wilt development on Chrysanthemum. *Environ. Sci Technol*. 2021 Jul 15; 55(15): 10805-10. <https://doi.org/10.3390/plants12030491>.
28. Muthukrishnan L. Nanotechnology for cleaner leather production: a review. *Environ Chem Lett*. 2021 :1-23. <https://doi.org/10.1016/j.asej.2018.08.001>.
29. Chowdhary P, Bharagava RN, Mishra S, Khan N. Role of industries in water scarcity and its adverse effects on environment and human health. *Environmental Concerns and Sustainable Development: Air, Water and Energy Resources*. 2020; 1: 235-56. https://doi.org/10.1007/978-981-13-5889-0_12.
30. Kansal SK, Kumari A. Potential of *M. oleifera* for the treatment of water and wastewater. *Chem Rev* 2014 May 14; 114(9): 4993-5010. <https://doi.org/10.1021/cr400093w>.
31. Saleh IA, Zouari N, Al-Ghouti MA. Removal of pesticides from water and wastewater: Chemical, physical and biological treatment approaches. *Environ Technol Innov*. 2020; 101026. <https://doi.org/10.1016/j.eti.2020.101026>.
32. Shah I, Adnan R. A Comprehensive review on the hierarchical performances of eco-friendly and functionally advanced modified and recyclable carbon materials. *J Iran Chem Soc*. 2020; 17(7): 1521-1537. <https://doi.org/10.1007/s13738-020-01900-7>.

33. Heidarinejad Z, Dehghani MH, Heidari M, Javedan G, Ali I, Sillanpää M. Methods for preparation and activation of activated carbon: a review *Environ. Chem Lett.* 2020; 18(2): 393-415. <https://doi.org/10.1007/s10311-019-00955-0>.
34. Hasanin M, Hashem AH, Lashin I, Hassan SA. In vitro improvement and rooting of banana plantlets using antifungal nanocomposite based on mycosynthesized copper oxide nanoparticles and starch. *Biomass Convers. Biorefinery.* 2021 Aug 6:1-1. <https://doi.org/10.1007/s13399-021-01784-4>.
35. Nguyen CH, Tran HN, Fu CC, Lu YT, Juang RS. Roles of adsorption and photocatalysis in removing organic pollutants from water by activated carbon-supported titania composites: Kinetic aspects. *J Taiwan Inst Chem Eng.* 2020 Apr 1; 109:51-61. <https://doi.org/10.1016/j.jtice.2020.02.019>.
36. Zhang H, Nengzi LC, Wang Z, Zhang X, Li B, Cheng X. Construction of Bi₂O₃/CuNiFe LDHs composite and its enhanced photocatalytic degradation of lomefloxacin with persulfate under simulated sunlight. *J Hazard Mater.* 2020; 383:121236. <https://doi.org/10.1016/j.jhazmat.2019.121236>.
37. Dhahir SA, Abdul-Hussein E, Sarhan ST, Faraj N. Adsorption of malachite green dye from aqueous solution onto Iraqi raw Al-Hussainiyat clay. *Eur Chem Bull.* 2013; 2(11): 866-72. <https://api.semanticscholar.org/CorpusID:55217037>.
38. Akintelu SA, Folorunso AS, Folorunso FA, Oyebamiji AK. Green synthesis of copper oxide nanoparticles for biomedical application and environmental remediation. *Heliyon.* 2020 Jul 1; 6(7):e04508. <https://doi.org/10.1016/j.heliyon.2020.e04508>.
39. Adel M, Ahmed MA, Mohamed AA. Effective removal of indigo carmine dye from wastewaters by adsorption onto mesoporous magnesium ferrite nanoparticles. *Environ Nanotechnol Monit Manag* 2021 Dec 1; 16: 100550. <https://doi.org/10.1016/j.enmm.2021.100550>.
40. Borth KW, Galdino CW, de Carvalho Teixeira V, Anaissi FJ. Iron oxide nanoparticles obtained from steel waste recycling as a green alternative for Congo red dye fast adsorption. *Appl Surf Sci.* 2021 Apr 30; 546: 149126. <https://doi.org/10.1016/j.apsusc.2021.149126>.
41. Aboud NA A, Jasim B E, Rheima AM. Methylene Orange dye removal in aqueous solution using synthesized CdO-MnO₂ nanocomposite: kinetic and thermodynamic studies. *Chalcogenide Lett.* 2021; 18(5): 237-243. <https://www.researchgate.net/publication/355758313>.
42. BENTONITE DO, TIO MB, ZNO A. Adsorption study of rhodamin B dye on Iraqi bentonite and modified bentonite by nanocompounds TiO₂, ZnO, AL₂O₃ and sodium dodecyl sulfate. *Amn Jn Environn Sci.* 2013; 9(3): 269-79. <http://www.thescipub.com/ajes.toc>.
43. Kumar KY, Muralidhara HB, Nayaka YA, Balasubramanyam J, Hanumanthappa H. Low-cost synthesis of metal oxide nanoparticles and their application in adsorption of commercial dye and heavy metal ion in aqueous solution. *Powder technol.* 2013 Sep 1; 246: 125-36. <https://doi.org/10.1016/j.powtec.2013.05.017>.
44. Farhan AM, Zaghair AM, Abdullah HI. Adsorption Study of Rhodamine-B Dye on Plant (Citrus Leaves). *Baghdad Sci J.* 2022; 19(4): 0838. <http://dx.doi.org/10.21123/bsj.2022.19.4.0838>.

قابلية امتزاز صبغة السايبيكرون الحمراء من محلولها المائي باستخدام دقائق أكسيد النحاس النانوية

آية قاسم خنجر¹، أحلام محمد فرحان¹، أحمد مهدي رحيمة²

¹قسم الكيمياء، كلية العلوم للبنات، جامعة بغداد، واسط، العراق.
²قسم الكيمياء، كلية العلوم، الجامعة المستنصرية، بغداد، العراق.

الخلاصة

يصف هذا البحث الإنتاج الصديق للبيئة لجسيمات النحاس النانوية باستخدام مستخلص نبات الجرجير والحرث عند درجة حرارة 400 درجة مئوية لمدة 3 ساعات. تم استخدام SEM و TEM لتحليل حجم الجسيمات النانوية المحضرة. تم استخدام حيود الأشعة السينية لتحديد الهيكل البلوري. كشف التحليل الطيفي للأشعة السينية المشتتة للطاقة لهيكل المنتج الذي تم إنشاؤه عن مكونات النحاس والأكسجين فقط، مما يدل على نقاء المادة المحضرة. استخدمت المادة النانوية المحضرة CuO NPs في امتزاز صبغة Cibacron الحمراء. في 35 دقيقة من زمن الاتزان، لوحظ امتزاز أسرع لصبغة Cibacron الحمراء على الجسيمات النانوية CuO. كان نموذجاً Freundlich و pseudo-second ذات قيم R^2 أكثر من 0.9785 و 0.999 على التوالي، الأكثر فاعلية في وصف عملية الامتزاز. تم حساب المعلمات ΔG , ΔH , ΔS . يمكن الاستنتاج أن CuO NPs هي سطح ممتاز فعال لصبغة Cibacron الحمراء.

الكلمات المفتاحية: الامتزاز، صبغة السايبيكرون الحمراء، أكسيد نحاس النانوي، التحليل الطيفي للأشعة السينية، التوليف الأخضر.